Journal of GeoEngineering, Vol. 15, No. 4, pp. 183-193, December 2020
http://dx.doi.org/10.6310/jog.202012_15(4).2

EFFECTS OF STRENGTH NONHOMOGENEITY AND NON-SATURATION ON STABILITY OF A 3D SLOPE

Zhaohui Pang [1] and Danping Gu [2*]

ABSTRACT

Soils are usually assumed to be homogeneous and dry/saturated in slope stability analyses most commonly. However, soils are actually nonmomogeneous and unsaturated commonly because of natural and man-made reasons. Cohesion nonhomogeneity and matric suction leads to a great difference of the shear strength of unsaturated soils from those of dry or saturated soils, resulting in quite a distinct stability condition. Based on limit analysis, the present study conducts a stability analysis of a three-dimensional (3D) slope in nonhomogeneous and unsaturated soils under steady flow. The external work rate by apparent cohesion is calculated using the variable-step Simpson method, thereafter the analytical expressions of required cohesion and the stability number of slope are derived from the energy balance equation, and consequently optimized solutions of the objectives are captured. Comparison is made to validate the present study, thereafter a parametric analysis is performed to explore the effects of soil cohesion nonhomogeneity, steady flow conditions, the air-entry pressure and 3D characteristics of slope on slope stability in different kinds of soils. The results indicate that slope stability is closely related to infiltration rate and cohesion nonhomogeneity, and there is a marked difference between 3D analysis and 2D analysis.

Key words: Unsaturated soils, 3D slope stability, cohesion nonhomogeneity, steady flow, infiltration rate.

1. INTRODUCTION

Slope stability analysis, a classical topic in geotechnical engineering, has mostly been conducted under two-dimensional (2D) conditions and the assumption that soils are homogeneous and dry/saturated (Stianson *et al*. 2015; Chen *et al*. 2017; Qin and Chian 2018; Li and Yang 2019). However, real soils are nonhomogeneous and unsaturated due to natural reasons such as deposition, compaction, rainfall, etc. Cohesion nonhomogeneity and matric suction make the shear strength of soils greatly different from the shear strength of homogeneous and dry/saturated soils, resulting in quite a distinct stability condition (Chen 1975; Han *et al*. 2014; Oh and Lu 2015; Qi and Vanapalli 2015; Vahedifard *et al*. 2015; Vahedifard *et al*. 2016). In addition, the failure of slopes typically has three-dimensional (3D) feature, and slope stability analysis under plane strain often results in conservative estimations (Lim *et al*. 2016; Michalowski and Drescher 2009; Michalowski and Nadukuru 2013; Xu and Yang 2018).

A series of investigations has been conducted to explore stability of slopes and earth retaining walls in either nonhomogeneous or unsaturated soils. However, mostly of them were conducted under 2D plane strain (Lu and Godt 2008; Nian *et al*. 2008; Zhang *et al*. 2014; Vahedifard *et al*. 2015; Vahedifard *et al*. 2016).

With respect to the investigations of stability of slopes in nonhomogeneous soils, the limit analysis method is an effective approach to deal with the slope stability issues. With regard to slope stability analysis of slopes in nonhomogeneous soils, Chen (1975) performed a stability analysis of a two-stage slope in nonhomogeneous soils, and the effect of cohesion nonhomogeneity on slope stability was investigated. Farzaneh and Askari (2003) used a numerical approach to analyze the upper bound stability of 3D slopes composed of nonhomogeneous soils under three kinds of failure mechanisms. They also proposed an iterative algorithm to obtain the optimized stability factors. Nian *et al.* (2008) conducted an upper bound stability analysis of a pile-reinforced slope in nonhomogeneous slope, and the effects of soil strength nonhomogeneity and pile location on slope stability were analyzed. Han *et al.* (2014) conducted a stability analysis of 3D slope subjected to surcharge loading, and the effects of parameters of interest, such as the soil strength nonhomogeneity, anisotropy and surcharge loading, on slope stability were investigated. Yang and Xu (2017) analyzed the stability of a 3D two-stage slope, and the stability of slopes under both the seismic and static conditions were investigated. Xu and Yang (2018a; 2018b) investigated the stability of pile-reinforced slope and geosynthetic-reinforced slopes, the optimal position for piles and the best geosynthetic reinforcement pattern for slope stability were obtained. A series of numerical solutions and stability charts were also proposed for preliminary design purposes.

The aforementioned investigations were mainly conducted under plane strain. However, it has been proved that 3D characteristics play a dominant role on slope stability. With regard to stability analysis of 3D slopes using the upper bound theorem of limit analysis, Michalowski and Drescher (2009) firstly proposed a 3D rotational failure mechanism to investigate the stability of 3D slopes. The analytical expression of the stability factor was proposed, and a series of numerical solutions of the stability factor were presented. The studies revealed that stability of slopes in three-dimension is of significant importance, especially for slopes with a smaller width-to-height ratio. Thereafter, based on

Manuscript received April 24, 2020; revised August 20, 2020; accepted August 11, 2020.
[1] Professor, College of Construction Engineering and Arts, Hunan Institute of Technology, Hengyang 421002, China.
[2*] Ph.D. (corresponding author), School of Civil Engineering, Changsha University of Science and Technology, Changsha, 410114; School of Civil Engineering, Changsha University of Science and Technology, Changsha, 410114, China (e-mail: danping_gu_2019@163.com).

the proposed 3D horn-like failure mechanism, a great amount of effort had been devoted to analyze the stability of 3D slopes. Based on the proposed 3D failure mechanism, Michalowski and Martel (2011) proposed a series of stability charts of 3D slopes subjected to seismic excitation for preliminary design purposes. Gao *et al.* (2013) extended the proposed 3D failure mechanism by Michalowski and Drescher (2009) to three different models, *i.e.,* the face failure, the base failure and toe failure, and a series of stability charts of slopes based on the three modified failure mechanisms was proposed. Gao *et al.* (2015) investigated the stability of 3D slopes following the nonlinear failure criterion, the critical height of slopes under both the nonlinear and linear criterions were compared. Yang (2018) conducted a stability analysis of 3D slope subjected to pore water pressure following the nonlinear failure criterion, and the effects of pore water coefficient and 3D characteristics on slope stability were analyzed.

With respect to slope stability in unsaturated soils, a number of investigations has been performed experimentally and numerically to investigate the shear strength of unsaturated soils and stability of geotechnical structures. Fredlund *et al.* (1978) firstly proposed an equation in terms of the Mohr-Coulomb failure criterion to calculate the shear strength of unsaturated soils. Thereafter, a set of formulas was reported by a number of scholars to estimate shear strength of unsaturated soils (Fredlund *et al.* 1996; Vanapalli *et al.* 1996; Khalili and Khabbaz 1998; Vilar 2006). One of the most representative formulas among the aforementioned equations is the extended Mohr-Coulomb equation proposed by Fredlund *et al.* (1978), in which the shear strength of unsaturated soil increases linearly with matric suction at the rate of tan φ^b, and φ^b, the suction angle, was a constant (φ^b = 15°). However, it was found later that φ^b was a variable and the relationship between shear strength and matric suction was nonlinear (Fredlund *et al.* 1996; Vahedifard *et al.* 2016). Consequently, Lu and Godt (2008) proposed a unified representation to take into account the effective stress of unsaturated soils. Based on the effective stress-based equation by Lu and Godt (2008), Vahedifard *et al.* (2016) conducted a limit-equilibrium analysis of a 2D slope in unsaturated soils, a parametric analysis was conducted to explore the effects of suction stress, soil types and infiltration on both stability and failure configuration of slopes, and a set of stability charts were presented for general use. Based on limit analysis, Li and Yang (2018) performed a 3D stability analysis of slope in unsaturated soils, the effects of 3D characteristics of slope, soil type and infiltration rate on stability of slope were explored.

Cohesion nonhomogeneity and soil strength unsaturation are key factors which affects slope stability significantly. As a consequence, the question, which has both theoretical and practical importance, is how to estimate the stability of a 3D slope in nonhomogeneous and unsaturated soils subjected to steady flow. To the authors' best knowledge, this issue has never been reported yet.

Consequently, in virtue of the kinematical approach of limit analysis (Huang *et al.* 2017; Pan *et al.* 2017; Huang *et al.* 2018; Pan and Dias 2018), a stability analysis of a 3D slope in nonhomogeneous and unsaturated soils subjected to various steady flow conditions is conducted in the present work. Based on the 3D rotational failure mechanism proposed by Michalowski and Drescher (2009), the work rate by apparent cohesion is calculated with the help of the variable-step Simpson method, thereafter the analytical expressions of the required cohesion and the stability number are derived. Comparison is made to verify the present work and a parametric analysis is performed to investigate the effects of cohesion nonhomogeneity, infiltration rate, internal friction angle, the air-entry pressure and 3D characteristics of slope on slope stability. Upper bound solutions of the stability numbers of slopes in different kinds of soils subjected to various steady flow conditions are presented for preliminary design purposes.

2. COHESION NONHOMOGENEITY AND APPARENT COHESION

2.1 Cohesion Nonhomogeneity

Cohesion nonhomogeneity for a slope in soils is calculated by the linear increasing of cohesion from $n_0 \times c$ on crest of slope to c at the base of slope, as shown in Fig. 1(b), cohesion c_h of soil at depth h is:

$$c_h = n_0\, c + \frac{(1-n_0)c}{H} h \tag{1}$$

where n_0 is the nonhomogeneity coefficient (Han *et al.* 2014), and soil is homogeneous when n_0 = 1.0. H in Eq. (1) means the slope height.

2.2 Apparent Cohesion of Unsaturated Soils

Based on the suction stress characteristic curve (SSCC), the effective stress σ' of soil can be expressed as (Lu and Godt 2008):

$$\sigma' = \sigma - u_a - \sigma^s \tag{2}$$

where σ denotes the total stress, u_a denotes the pore-air pressure; for unsaturated soils, σ^s can be expressed as:

$$\sigma^s = -\frac{(u_a - u_w)}{\left\{1.0 + \left[\alpha(u_a - u_w)\right]^n\right\}^{(n-1)/n}} \tag{3}$$

where $(u_a - u_w) > 0$ denotes the matric suction in unsaturated soils, u_w denotes the pore-water pressure; α = (0.001 ~ 0.5) kPa^{-1} is approximately the inverse of the air-entry pressure, and n = 1.1 ~ 8.5 denotes a fitting parameters referring the breadth of the pore size of soil, depending on the soil type. Detailed value ranges for α and n are listed in Table 1.

Table 1 Values of α and n concerning various soils from Vahedifard *et al.* (2015)

Soil type	α (kPa^{-1})	n
Sandy clay	0.001 ~ 0.01	4.0 ~ 8.5
Sandy silt	0.01 ~ 0.1	4.0 ~ 8.5
Sand	0.1 ~ 0.5	4.0 ~ 8.5
Silty clay	0.001 ~ 0.01	2.0 ~ 4.0
Silt	0.01 ~ 0.1	2.0 ~ 4.0
Silty sand	0.1 ~ 0.5	2.0 ~ 4.0
Clay	0.001 ~ 0.01	1.1 ~ 2.5
Clayey silt	0.01 ~ 0.1	1.1 ~ 2.5
Clayey sand	0.1 ~ 0.5	1.1 ~ 2.5

In the present study, four different kinds of soils are considered, and their strength parameters are listed in Table 2. In Table 2, k_s denotes the saturated hydraulic conductivity.

Table 2 Strength parameters concerning different kinds of soils from Vahedifard *et al.* (2015)

Soil type	n	α (kPa^{-1})	k_s (m/s)
Clay	2	0.005	5×10^{-8}
Silt	3	0.01	5×10^{-7}
Loess	4	0.025	1×10^{-6}
Sand	5	0.1	3×10^{-5}

The matric suction ($u_a - u_w$) of unsaturated soil subjected to steady flow can be expressed as follows (Gardner 1958; Vahedifard *et al.* 2016):

$$(u_a - u_w) = -\frac{1}{\alpha}\ln\left[\left(1+\frac{q}{k_s}\right)e^{-\gamma_w \alpha z} - \frac{q}{k_s}\right] \tag{4}$$

where in Eq. (4), γ_w denotes water unit weight; z denotes the vertical distance between a point in soil mass and water table, and $(u_a - u_w) = 0$ at $z = 0$; q (m/s) denotes vertical specific discharge, and $q > 0$, $q < 0$ and $q = 0$ denote evaporation, infiltration and a no-flow case, respectively.

Combining Eqs. (3) and (4), apparent cohesion c_{app} of unsaturated soil due to matric suction can be expressed as:

$$c_{app} = -\frac{1}{\alpha}\tan\varphi \frac{\ln\left[\left(1+\frac{q}{k_s}\right)e^{-\gamma_w\alpha z} - \frac{q}{k_s}\right]}{\left(1+\left\{-\ln\left[\left(1+\frac{q}{k_s}\right)e^{-\gamma_w\alpha z} - \frac{q}{k_s}\right]\right\}^n\right)^{(n-1)/n}} \tag{5}$$

where φ is the effective friction angle of soil. Besides, when it comes to the 3D rotational failure mechanism and to the insert plane, the symbol z in Eq. (5) becomes z_{3D} and z_{2D}, as expressed in Eqs. (17) and (18), respectively.

3. LIMIT ANALYSIS AND FAILURE MECHANISM OF A 3D SLOPE

3.1 Upper Bound Theorem of Limit Analysis

The upper bound theorem of limit analysis is an effective approach to analyze slope stability issues. The kinematic approach of upper bound theorem of limit analysis states that the internal dissipation rate is not less than the work rate of body force, namely

$$\int_V \sigma_{ij}^* \dot{\varepsilon}_{ij}^* \, dV \geq \int_S T_i \, v_i \, dS + \int_V X_i \, v_i^* \, dV \tag{6}$$

where $\dot{\varepsilon}_{ij}^*$ and σ_{ij}^* are strain rate and stress, respectively; v_i is the velocity along the failure surface; v_i^* is the velocity vector of a soil element in the failure mechanism on boundary S; V is the volume. More detailed explanation on the limit analysis method can be found in Chen (1975) and Michalowski and Drescher (2009).

3.2 Failure Mechanism of a 3D Slope

The 3D rotational failure mechanism of slope has the shape of spiral conic with a vertex angle of 2φ, as illustrated in Fig. 1(a). The height and angle of slope are denoted by H and β, respectively; the vertical distance between slope toe and the water table is z_0. The failure surface of slope rotates along the rotation center O from OA to OC, as shown in Fig.1(a). Physical meanings of other symbols can also be found in Fig. 1(a).

The two logarithmic spirals, AC and $A'C'$ are:

$$AC = r_0 \, e^{(\theta-\theta_0)\tan\varphi} \tag{7}$$

and

$$A'C' = r_0' \, e^{-(\theta-\theta_0)\tan\varphi} \tag{8}$$

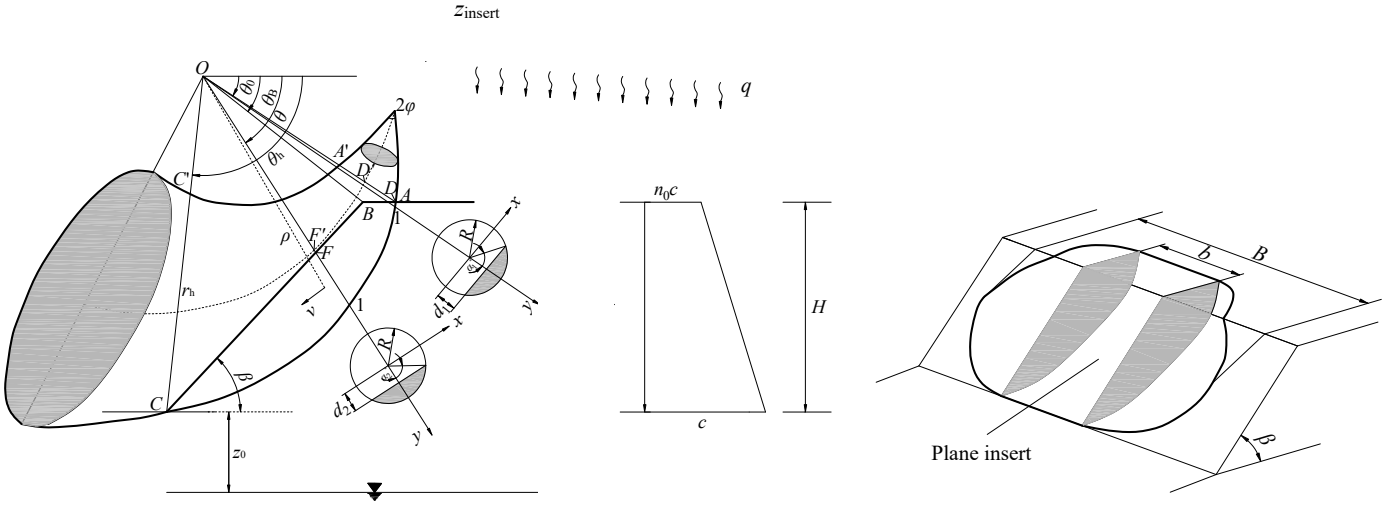

(a) 3D rotational failure mechanism of slope (b) Cohesion nonhomogeneity (c) 3D failure mechanism of slope with plane insert

Fig. 1 3D rotational failure mechanism and cohesion nnhomogeneity of slope subjected to steady flow

According to the geometrical relationship illustrated in Fig. 1(a), the distance between point O and the axis of r_m and the radius of a cross-section R can be expressed as

$$r_m = (r + r')/2 = r_0 f_1 \tag{9}$$

$$R = (r - r')/2 = r_0 f_2 \tag{10}$$

where f_1 and f_2 can be found in Eqs. (A1) and (A2) in the Appendix A.

According to Fig. 1(a), shape of the failure mechanism of slope can be determined by r_0'/r_0, θ_0 and θ_h. Additionally, it is clarified by investigations that slope stability is also related to the width of slope, thus a plane of width b is inserted into the symmetry plane of the 3D failure mechanism to make the total width of the failure mechanism to B, as shown in Fig. 1(c). The 3D failure mechanism will degenerate to 2D when $b \to \infty$.

4. WORK RATE CALCULATION

4.1 Internal Energy Dissipation by Soil Cohesion

The internal energy dissipation by soil cohesion on the 3D rotational failure mechanism in nonhomogeneous soil is:

$$\begin{aligned} D_{c\_\text{AB-3}D} &= 2\omega \int_{\theta_0}^{\theta_B} \int_0^{\alpha_1^*} c(\theta)\, R(r_\text{m} + R\cos\alpha)^2 d\alpha d\theta \\ &= \omega n_0 c r_0^3 g_1 + \omega \frac{1-n_0}{H} c r_0^4 g_2 \end{aligned} \tag{11}$$

$$\begin{aligned} D_{c\_\text{BC-3}D} &= 2\omega \int_{\theta_B}^{\theta_C} \int_0^{\alpha_2^*} c(\theta)\, R(r_m + R\cos\alpha)^2 d\alpha d\theta \\ &= \omega n_0 c r_0^3 g_3 + \omega \frac{1-n_0}{H} c r_0^4 (g_4 + g_5) \end{aligned} \tag{12}$$

where $D_{c\_\text{AB-3}D}$ and $D_{c\_\text{BC-3}D}$ are the internal energy dissipations along section $\theta_0 \sim \theta_B$ and section $\theta_B \sim \theta_h$, respectively; $\alpha_1^* = \arccos(d_1/R)$, $\alpha_2^* = \arccos(d_2/R)$, $d_1 = r_0 f_3$, $d_2 = r_0 f_4$.

The internal energy dissipation by soil cohesion of the inserted block is:

$$D_{c\_\text{insert}} = b \int_{S_t} c\cos\varphi [v]\, dS_t = \omega n_0 c r_0^3 g_6 + \omega \frac{1-n_0}{H} c r_0^4 g_7 \tag{13}$$

Thus, D_{int_c}, the total internal energy dissipation by soil cohesion is:

$$\begin{aligned} D_{\text{int}\_c} &= D_{c\_3D} + D_{c\_\text{insert}} = \omega n_0 c r_0^3 (g_1 + g_3 + g_6) \\ &\quad + \omega \frac{1-n_0}{H} c r_0^4 (g_2 + g_4 + g_5 + g_7) \end{aligned} \tag{14}$$

where g_1 to g_7 are as given in Eqs. (A8) ~ (A14) in the Appendix A.

4.2 Internal Energy Dissipation by Apparent Cohesion

The internal energy dissipation by apparent cohesion on the 3D spiral conic rotational body can be expressed as:

$$\begin{aligned} D_{app\_3D} = 2\omega \Bigg[& \int_{\theta_0}^{\theta_B} \int_0^{\alpha_1^*} c_{app\_3D} R(r_m + R\cos\alpha)^2 d\alpha d\theta \\ & + \int_{\theta_B}^{\theta_h} \int_0^{\alpha_2^*} c_{app\_3D} R(r_m + R\cos\alpha)^2 d\alpha d\theta \Bigg] \end{aligned} \tag{15}$$

The internal energy dissipation by apparent cohesion on the insert block can be expressed as:

$$D_{app\_\text{insert}} = b \int_{\theta_0}^{\theta_h} c_{app\_\text{insert}} v r d\theta \tag{16}$$

where c_{app_3D} and c_{app_insert} can be calculated using Eq. (5). It should be noted that the symbol 'z' in Eq. (5) is z_{3D} and zinsert, respectively, when c_{app_3D} and c_{app_insert} are calculated, and the expressions of z_{3D} and z_insert are:

$$z_{3D} = r_h \sin\theta_h - r\sin\theta + R(1-\cos\alpha)\sin\theta + z_0 \tag{17}$$

$$z_\text{insert} = r_h \sin\theta_h - r\sin\theta + z_0 \tag{18}$$

Thus, the total work rate by apparent cohesion can be expressed as:

$$D_{app\_c} = D_{app-3D} + D_{app\_\text{insert}} \tag{19}$$

4.3 Work Rate by Soil Weight

Work rate by soil weight of the 3D rotational body can be expressed as:

$$\begin{aligned} W_{\gamma-3\text{D}} = 2\omega\gamma \Big[& \int_{\theta_0}^{\theta_\text{B}} \int_0^{x_1^*} \int_{d_1}^{y^*} (r_\text{m} + y)^2 \cos\theta dx dy d\theta \\ & + \int_{\theta_\text{B}}^{\theta_\text{h}} \int_0^{x_2^*} \int_{d_2}^{y^*} (r_\text{m} + y)^2 \cos\theta dx dy d\theta \Big] = \gamma\omega r_0^4 g_8 \end{aligned} \tag{20}$$

where $y^* = \sqrt{R^2 - x^2}$ and x is $x_i^* = \sqrt{R^2 - d_i^2}$ (i = 1, 2).

Work rate by soil weight of the insert block can be found in Chen (1975) as:

$$W_{\gamma-\text{insert}} = \gamma\omega r_0^4 g_9 \tag{21}$$

The total external work rate by soil weight is:

$$W_\gamma = W_{\gamma-3\text{D}} + W_{\gamma-\text{insert}} = \gamma\omega r_0^4 (g_8 + g_9) \tag{22}$$

where g_8 and g_9 are given in Eqs. (A15) and (A16) in the Appendix A.

4.4 Energy Balance Equation

By equating the external work rate to the internal energy, the energy balance equation of a 3D slope under steady flow is expressed as follows:

$$W_\gamma = D_{\text{int}\_c} + D_{app\_c} \tag{23}$$

4.5 Required Cohesion and Stability Number

By solving the energy balance equation, the required cohesion c of slope can be expressed as:

$$c = \frac{W_\gamma - (D_{\text{int}\_c} + D_{app\_c})}{\omega n_0 r_0^3 (g_1 + g_3 + g_6) + \omega \frac{1-n_0}{H} r_0^4 (g_2 + g_4 + g_5 + g_7)} \tag{24}$$

Consequently, the stability number N_s can be written as:

$$N_s = c'/\gamma H \tag{25}$$

where c' is the maximum required cohesion to produce a limit equilibrium state of slope.

The constraint condition can be obtained from the geometry relationship shown in Fig. 1 to capture the required cohesion and stability number of slope:

$$\begin{cases} 0 < \theta_0 < \theta_B < \theta_h < \pi \\ 0 < r_0'/r_0 < 1 \\ 0 < (b + B'_{\max})/H < B/H \end{cases} \tag{26}$$

5. COMPARISON

Comparison is first made to verify the present study. As shown in Table 3, the required cohesion needed to produce a limit equilibrium state of slope in four different soils subjected to various steady flow conditions under B/H = 10.0 is captured and compared with the results by Vahedifard *et al.* (2016) under 2D plane strain. The parameters selected for optimization are $\beta = 90°$ (a vertical slope), H = 5 m, γ = 20 kN/m^3, z_0 = 0 and n_0 = 1.0 (homogeneous condition).

It is clear from Table 3 that the present solutions are in good agreement with the results by Vahedifard *et al.* (2016), the maximum discrepancy between the present solutions and the results by Vahedifard *et al.* (2016) is less than 1%. In such a case, the present study can be validated.

6. PARAMETRIC ANALYSIS

A parametric analysis is performed to explore the effects of indexes α and n, soil type, slope height H, infiltration rate, cohesion nonhomogeneity, soil type, and 3D characteristics on slope stability. The parameters selected are as shown in the figures.

6.1 Effects of n versus $1/\alpha$ on N_s

Figure 2 is the illustration of the stability number N_s of slope under different coefficient n versus $1/\alpha$, under different slope height H and nonhomogeneity coefficient n_0. Other parameters are B/H = 1.0, $\beta = 90°$, $\varphi = 20°$, and q = 0 (no-flow condition), slope height H = 2.0 m in Fig. 2(a), 2(c), and 2(e); and H = 10.0 m in Fig. 2(b), 2(d), and 2(f). The nonhomogeneity coefficient n_0 = 0, 0.5, and 1.0 (the homogeneous condition) in Fig. 2(a), Fig. 2(c), and Fig. 2(e), and in Fig. 2(b), Fig. 2(d), and Fig. 2(f), respectively.

As shown in Fig. 2, parameters $1/\alpha$, H, n_0 and n all have significant influences on slope stability, for that the stability number N_s decreases with the increase of n_0 and the decrease of α. The impact of suction on slope stability becomes more significant with the increase of parameter n, for a slope with a given α, the stability number N_s gets greater with a higher n and then turns into a constant with the increase of $1/\alpha$. In addition, it is seen that the stability of a slope is closely related to the slope height H. For a slope with a lower slope height H, the stability number N_s decreases sharply with the increase of $1/\alpha$ firstly and then reaches a constant value asymptotically. However, when it comes to a slope with a greater H, the N_s curves along with $1/\alpha$ become relatively gentle, indicating that the impact of suction stress on slope stability is weaker than that for a slope with a lower height.

6.2 Effects of the Infiltration Rate versus B/H on N_s

Figure 3 is the illustration of the stability numbers under infiltration, evaporation, the no-flow condition and the no suction condition, respectively, versus B/H in clay, silt and loess, respectively. Parameters are H = 3 m, $\beta = 90°$, n_0 = 0, and B/H varies from 0.8 to 10.0.

It is shown in Fig. 3 that the stability number N_s increases significantly with the increase of ratio B/H, especially within the range $B/H \le 2.0$, indicating that the 3D characteristics of slope has a significant adverse effect on slope stability. This shows that 2D stability analysis will lead to conservative estimations, thus, it is clear that significant importance to investigate the stability of a slope in three-dimension. It is also indicated in Fig. 3 that a slope requires the lowest cohesion under evaporation ($q = 1.15 \times 10^{-8}$ m/s), the second lowest under no-flow condition, then under the infiltration and lastly under the no suction condition, meaning that a slope obtains the best stability condition under evaporation and the worst under the no-suction condition. In addition, it is also seen from Fig. 3 that the differences between the N_s solutions obtained under various steady flow conditions are more pronounced for slopes in clay and silt, but are negligible for slopes in loess, meaning that the steady flow condition should be carefully handled and measured for slopes in clay and silt.

6.3 Effects of Infiltration Rate versus n_0 on N_s

Figure 4 is the illustration of the stability numbers N_s of slope under infiltration, evaporation, the no-flow condition and the no suction condition, respectively, versus the nonhomogeneity coefficient n_0 in clay, silt, and loess, respectively. Parameters are B/H = 2.0, H = 3 m, $\beta = 90°$ and the nonhomogeneity coefficient n_0 varies from 0 to 1.0 (the homogeneous condition).

Table 3 Comparison of required cohesion (kPa) with the solutions by Vahedifard *et al.* (2016)

Soil types	φ (°)	Solutions	No suction	Infiltration $q = -3.14 \times 10^{-8}$ m/s	No-flow q = 0	Evaporation $q = 1.15 \times 10^{-8}$ m/s
Clay	20	Vahedifard *et al.* (2016)	18.2	15.3	10.1	8.2
		Present solution	18.15	15.21	10.06	8.13
Silt	25	Vahedifard *et al.* (2016)	16.5	7.0	6.4	6.1
		Present solution	16.46	7.03	6.35	6.10
Loess	28	Vahedifard *et al.* (2016)	15.6	6.8	6.7	6.7
		Present solution	15.51	6.76	6.70	6.68

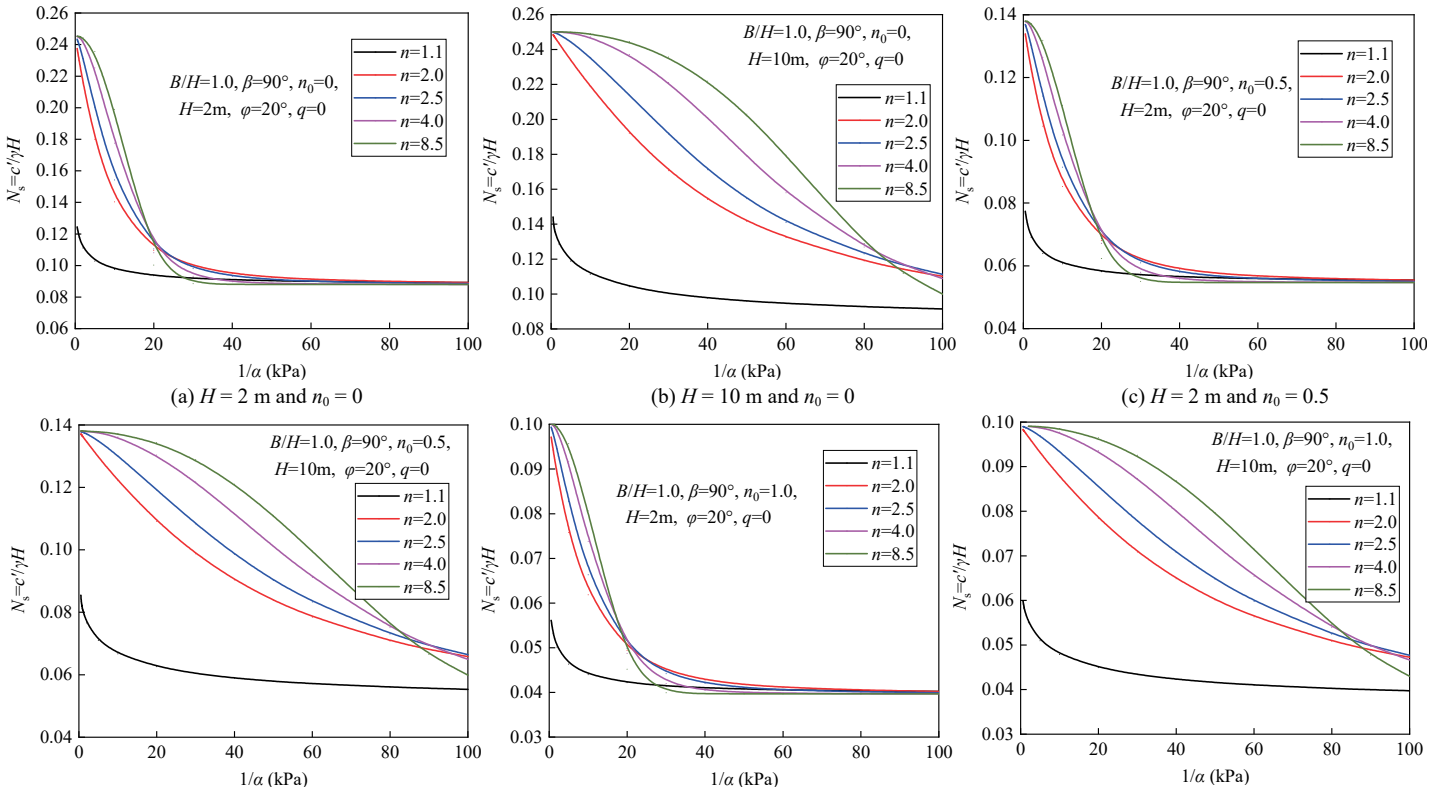

(a) H = 2 m and n_0 = 0 (b) H = 10 m and n_0 = 0 (c) H = 2 m and n_0 = 0.5

(d) H = 10 m and n_0 = 0.5 (e) H = 2 m and n_0 = 1.0 (the homogeneous condition) (f) H = 10 m and n_0 = 1.0 (the homogeneous condition)

Fig. 2 Effects of n on N_s versus 1/α with B/H = 1.0, β = 90°, φ = 20°, q = 0 with different conditions

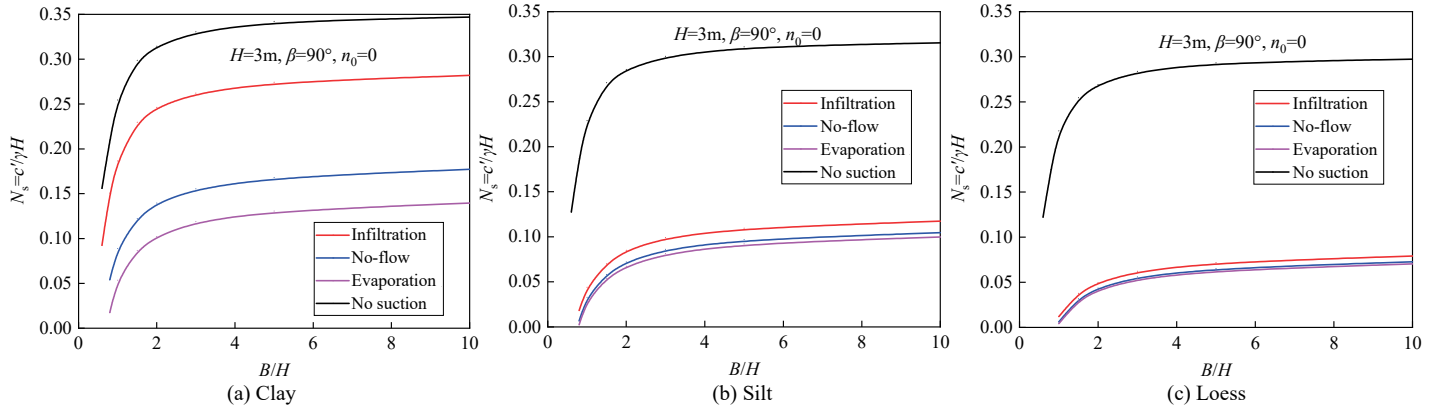

(a) Clay (b) Silt (c) Loess

Fig. 3 Effects of infiltration rate on N_s versus B/H in different soils

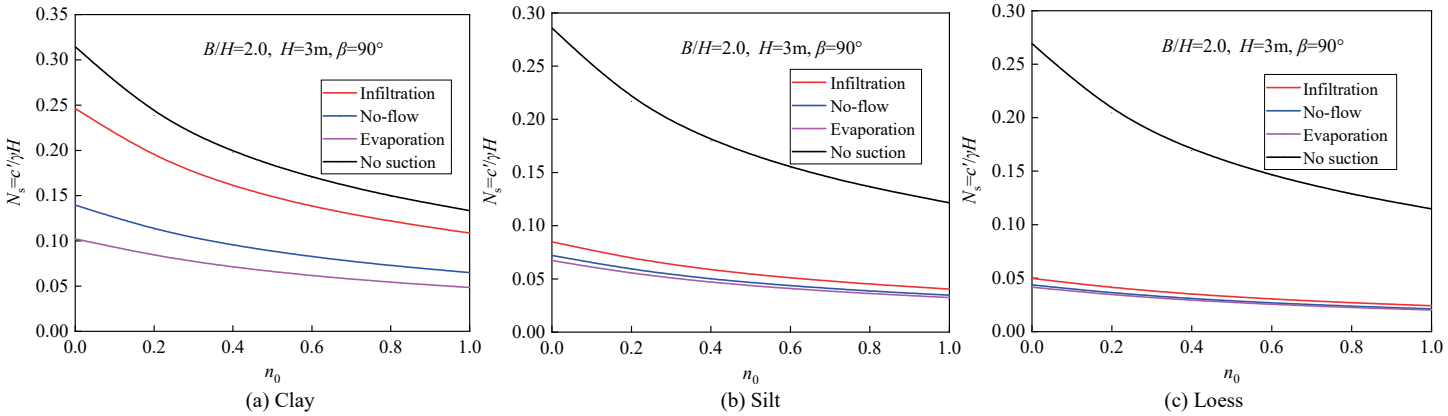

(a) Clay (b) Silt (c) Loess

Fig. 4 Effects of infiltration rate on N_s versus n_0 in different soils

As shown in Fig. 4, the stability number N_s decreases with the increase of n_0, indicating that increase of n_0 is beneficial for slope stability in nonhomogeneous soils. It is also seen from Fig. 4 that when n_0 increases from 0 to 1.0, the stability number N_s decreases 55.89%, 53.44%, 52.60%, and 57.55%, respectively, under the infiltration, the no-flow condition, evaporation and the no suction condition for a slope in clay. This means that cohesion nonhomogeneity has a significant effect on slope stability, especially for slopes in clay and silt. However, stability condition of slopes in loess is barely influenced by the infiltration rate, which is in accordance with the findings from Fig. 3.

6.4 Effects of Cohesion Nonhomogeneity versus 3D Characteristics of Slope on N_s

Figure 5 is the illustration of the stability number under different nonhomogeneity coefficient n_0 versus ratio B/H in clay, silt, and loess, respectively. Parameters are H = 3 m, β = 90°, q = 0 (no-flow condition), the nonhomogeneity coefficient n_0 varies from 0 to 1.0, and ratio B/H varies from 0.8 to 10.0.

It is clear from Fig. 5 that the stability number N_s decreases with the increase of n_0, which means increase of n_0 is beneficial for slope stability. More specifically, for a slope under B/H = 10.0, the stability number N_s decreases more than 50% when the nonhomogeneity coefficient n_0 increases from 0 to 1.0, indicating that cohesion nonhomogeneity has an important impact on slope stability. However, it is also clear from Fig. 5 that the rules of N_s along with ratio B/H under different n_0 are basically the same, which means the nonhomogeneity coefficient n_0 will only influence the stability number, but barely change the rules of ratio B/H on slope stability.

6.5 Effects of Soil Type versus n_0 and φ on N_s

Figure 6 is the illustration of the stability numbers N_s of slope in clay, silt, and loess, respectively, versus the nonhomogeneity coefficient n_0 and the internal friction angle φ. Parameters chosen are as shown in each figure.

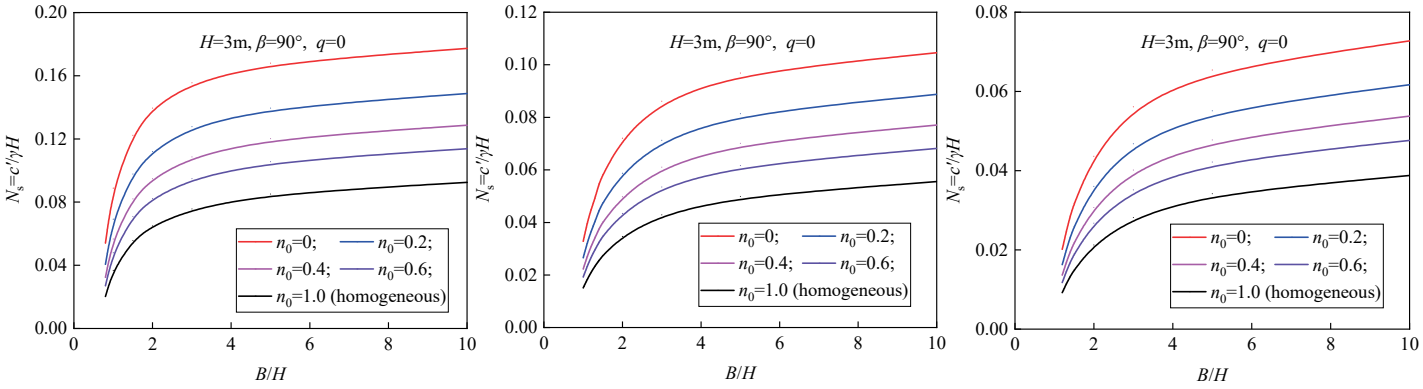

Fig. 5 Effect of n_0 on N_s versus B/H in different soils

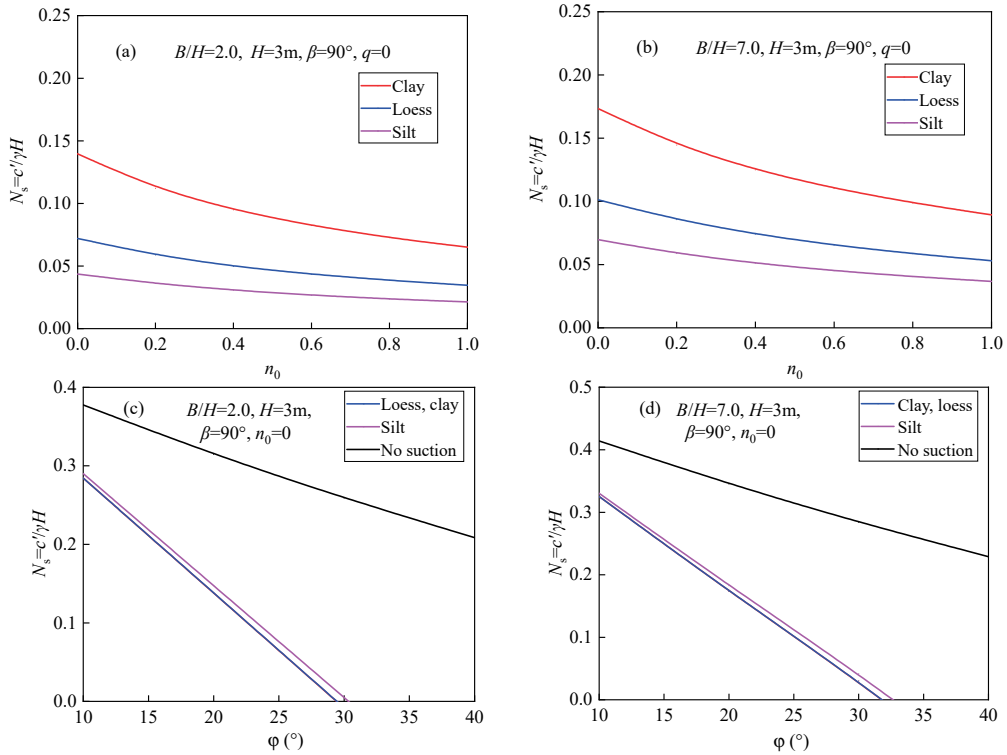

Fig. 6 Effects of soil type on N_s: (a) B/H = 2.0, versus n_0; (b) B/H = 7.0, versus n_0; (c) B/H = 2.0, versus φ; (d) B/H = 7.0, versus φ

As shown in Figs. 6(a) and 6(b), the stability number N_s decreases 53.44% and 51.85%, respectively, for a 3D slope with B/H = 2.0 in clay, and loess when the nonhomogeneity coefficient n_0 increases from 0 to 1.0, while decreases 52.87%, 48.48%, and 47.62%, respectively, for a slope with B/H = 7.0 in the four kinds of soils. This means that 3D characteristics of slope will influence the impacts of cohesion nonhomogeneity on slope stability. From Figs. 6(c) and 6(d), it is seen that N_s decreases linearly with the increase of the internal friction angle φ, meaning that φ has a favorable impact on slope stability, and the variation of ratio B/H barely change the influencing rules of the internal friction angle φ on slope stability.

7. NUMERICAL SOLUTIONS

Four sets of numerical solutions of the stability number N_s of a vertical slope (β = 90°) in clay, silt, and loess subjected to infiltration, no-flow, evaporation and the no suction condition are presented in Table 3 through Table 6. In these tables, the nonhomogeneity coefficient n_0 varies from 0 to 1.0 (the homogeneous condition), and B/H changes from 0.8 to 10.0 (2D plane strain). The numerical solutions can be easily used to obtain the stability number N_s of a 3D slope in different soils subjected to various steady flow conditions. These tables will be helpful for preliminary design of slopes.

8. CONCLUSIONS

In the present work, the upper bound theorem of limit analysis is employed to investigate the stability of 3D slope in different nonhomogeneous and unsaturated soils subjected to various steady flow conditions. The external work rate by apparent cohesion is calculated in virtue of the variable-step Simpson method. The analytical expressions of required cohesion and stability number of slope are obtained based on the energy balance equation. Comparison is made to verify the present work, and a parametric analysis is conducted to investigate the effects of cohesion nonhomogeneity, infiltration rate, the air-entry pressure, and the 3D characteristics of slope on slope stability. Numerical solutions are given at the end of the paper for preliminary design purposes. The following conclusions can be drawn:

1. Infiltration rate impacts slope stability significantly. A slope obtains a better stability condition under evaporation and the worst under the no-suction condition. The differences between the stability factors obtained under the different steady flow conditions are pronounced for slopes in clay and silt, but are negligible for slopes in loess, meaning that infiltration rate should be carefully measured for a slope in clay and silt.

Table 4 Stability number N_s (× 10^{-2}) of a vertical (β = 90°) 3D nonhomogeneous slope in clay subjected to various steady flow conditions

Steady flow condition	B/H	n_0					
		0	0.2	0.4	0.6	0.8	1.0
Infiltration	0.8	15.07	11.29	9.03	7.53	6.45	5.64
	1	18.66	14.17	11.60	9.81	8.54	7.57
	2	24.63	19.18	15.98	13.75	12.14	10.87
	5	27.43	22.29	18.95	16.55	14.74	13.30
	10	28.18	23.31	20.03	17.58	15.70	14.19
No-flow	0.8	5.41	4.06	3.24	2.70	2.32	2.03
	1	8.89	6.91	5.66	4.79	4.15	3.68
	2	13.96	11.21	9.49	8.23	7.26	6.50
	5	16.80	13.95	12.01	10.56	9.42	8.51
	10	17.73	14.88	12.87	11.38	10.21	9.26
Evaporation	0.8	1.76	1.32	1.06	0.88	0.75	0.66
	1	5.36	4.17	3.41	2.89	2.50	2.21
	2	10.23	8.36	7.08	6.14	5.42	4.85
	5	13.06	10.96	9.46	8.32	7.42	6.71
	10	13.96	11.81	10.27	9.09	8.16	7.40
No suction	0.8	20.99	15.56	12.77	10.83	9.40	8.30
	1	25.45	18.43	15.02	12.83	11.25	10.01
	2	31.45	23.84	19.74	16.97	14.91	13.35
	5	34.40	27.18	23.03	20.05	17.83	16.05
	10	34.69	28.27	24.17	21.19	18.89	17.08

Table 5 Stability number N_s (×10^{-2}) of a vertical (β = 90°) 3D nonhomogeneous slope in silt subjected to various steady flow conditions

Steady flow condition	B/H	n_0					
		0	0.2	0.4	0.6	0.8	1.0
Infiltration	0.8	1.82	1.43	1.18	1.0	0.87	0.77
	1	4.40	3.56	2.99	2.58	2.27	2.03
	2	8.49	6.89	5.84	5.08	4.51	4.05
	5	10.96	9.21	7.94	6.97	6.22	5.63
	10	11.74	9.96	8.65	7.64	6.85	6.22
No-flow	0.8	0.67	0.53	0.43	0.37	0.32	0.28
	1	3.29	2.66	2.23	1.93	1.69	1.52
	2	7.20	5.88	4.98	4.34	3.86	3.47
	5	9.69	8.14	7.01	6.16	5.51	4.99
	10	10.46	8.87	7.71	6.81	6.12	5.56
Evaporation	0.8	0.25	0.19	0.16	0.14	0.12	0.10
	1	2.88	2.33	1.96	1.69	1.48	1.33
	2	6.73	5.50	4.66	4.08	3.62	3.25
	5	9.22	7.74	6.67	5.87	5.25	4.76
	10	9.99	8.47	7.36	6.52	5.85	5.31
No suction	0.8	18.70	13.90	11.44	9.72	8.47	7.51
	1	22.90	16.63	13.54	11.59	10.19	9.11
	2	2.59	2.17	17.97	15.44	13.60	12.16
	5	31.09	24.73	20.94	18.26	16.21	14.61
	10	31.53	25.70	21.99	19.28	17.20	15.53

Table 6 Stability number N_s (×10^{-2}) of a vertical (β = 90°) 3D nonhomogeneous slope in loess subjected to various steady flow conditions

Steady flow condition	B/H	n_0					
		0	0.2	0.4	0.6	0.8	1.0
Infiltration	0.8	–	–	–	–	–	–
	1	1.19	0.96	0.80	0.69	0.61	0.54
	2	4.97	4.10	3.49	3.04	2.69	2.42
	5	7.19	6.03	5.23	4.61	4.13	3.74
	10	7.92	6.70	5.84	5.17	4.64	4.21
No-flow	0.8	–	–	–	–	–	–
	1	0.63	0.50	4.22	3.62	3.18	2.83
	2	4.36	3.60	3.07	2.67	2.37	2.13
	5	6.54	5.51	4.78	4.22	3.77	3.42
	10	7.27	6.17	5.38	4.76	4.27	3.88
Evaporation	0.8	–	–	–	–	–	–
	1	0.42	0.34	0.28	0.24	0.21	0.19
	2	4.15	3.43	2.92	2.54	2.25	2.02
	5	6.31	5.32	4.62	4.08	3.65	3.30
	10	7.04	5.98	5.21	4.62	4.14	3.76
No suction	0.8	17.51	12.85	10.67	9.15	8.01	7.12
	1	21.78	15.57	12.72	10.87	9.58	8.59
	2	26.94	20.44	16.93	14.57	12.82	11.47
	5	29.34	23.31	19.77	17.21	15.31	13.79
	10	29.74	24.25	20.74	18.18	16.21	14.65

2. Increase of the nonhomogeneity coefficient n_0 is beneficial for slope stability. The effects of cohesion nonhomogeneity on stability of slopes in different soils and under different steady flow conditions are different.
3. The stability number of slope increases with the increase of B/H, especially within $B/H \leq 2.0$, and there is a significant distinction between the stability factors obtained under a 3D condition and under 2D plane strain, and a 2D analysis obtains conservative estimations.
4. Impact of suction on slope stability becomes more significant with the increase of parameter n, and the stability number gets greater with a higher n for a slope with a given α. The stability of slope is closely related to slope height H, for a slope with a lower slope height H, the stability number N_s decreases sharply with the decrease of α firstly and then reaches a constant value asymptotically. However, when is comes to a slope with a greater H, N_s curves become relatively gentle along with $1/\alpha$, indicating that the impact of suction stress on slope stability is weaker than that for a slope with a lower height.

ACKNOWLEDGEMENTS

The author thanks the anonymous reviewers for the valuable comments and suggestions which have really helped to improve the paper.

FUNDING

This work was supported by the Planning project of Hunan Province (XJK17BGD013), the Scientific research project of department of education of Hunan Province (17C0439), the Scientific research project of Hengyang science and technology bureau (2016KG66), and the Research learning and innovative experimental project for college students in Hunan Province. The financial supports are greatly appreciated.

DATA AVAILABILITY

The data and/or computer codes used/generated in this study are available from the corresponding author on reasonable request.

CONFLICT OF INTEREST STATEMENT

The author(s) declare that there is no conflict of interest.

REFERENCES

Chen, C.S., Xia, Y.Y., and Bowa, V.M. (2017). "Slope stability analysis by polar slice method in rotational failure mechanism." *Computers and Geotechnics*, **81**, 188-194. https://dx.doi.org/10.1016/j.compgeo.2016.08.016 0266-352X

Chen, W.F. (1975). *Limit Analysis and Soil Plasticity*. Elsevier Science, Amsterdam.

Fredlund, D.G., Morgenstern, N.R., and Widger, R.A. (1978). "The shear strength of unsaturated soils." *Canadian Geotechnical Journal*, **15**(3), 313-321. https://doi.org/10.1139/t78-029

Fredlund, D.G., Xing, A., Fredlund, M.D., and Barbour, S.L. (1996). "The relationship of the unsaturated soil shear strength to the soil water characteristic curve." *Canadian Geotechnical Journal*, **32**(3), 440-448. https://doi.org/10.1139/t96-065

Gardner, W.R. (1958). "Some steady-state solutions of the unsaturated moisture flow equation with application to evaporation from a water table." *Soil Science*, **85**(4), 228-232. https://doi.org/10.1097/00010694-195804000-00006

Han, C.Y., Chen, J.J., and Xia, X.H. (2014). "Three-dimensional stability analysis of anisotropic and non-homogeneous slopes using limit analysis." *Journal of Central South University*, **21**(3), 1142-1147. https://doi.org/10.1007/s11771-014-2047-8

Huang, F, Ou, R.C., Li, Z.L., Yang, X.L., and Ling, T.H. (2018). "Limit analysis for the face stability of a shallow-shield tunnel based on a variational approach to the blow-out failure mode." *International Journal of Geomechanics*, ASCE, **18**(6), 04018038. https://doi.org/10.1061/(ASCE)GM.1943-5622.0001150

Huang, F., Zhao, L.H., Ling, T.H., and Yang, X.L. (2017). "Rock mass collapse mechanism of concealed karst cave beneath deep tunnel." *International Journal of Rock Mechanics and Mining Sciences*, **91**, 133-138. https://doi.org/10.1016/j.ijrmms.2016.11.017

Khalili, N. and Khabbaz, M.H. (1998). "A unique relationship for χ for the determination of the shear strength of unsaturated soils." *Géotechnique*, **48**(5), 681-687. https://doi.org/10.1680/geot.1998.48.5.681

Li, Y.X. and Yang, X.L. (2019). "Soil slope stability considering effect of soil strength nonlinearity." *International Journal of Geomechanics*, ASCE, **19**(3), 04018201. https://doi.org/10.1061/(ASCE)GM.1943-5622.0001355

Li, Z.W. and Yang, X.L. (2018). "Stability of 3D slope under steady unsaturated flow condition." *Engineering Geology*, **242**, 150-159. https://doi.org/10.1016/j.enggeo.2018.06.004

Lim, K., Lyamin, A.V., Cassidy, M.J., and Li, A.J. (2016). "Three-dimensional slope stability charts for frictional fill materials placed on purely cohesive clay." *International Journal of Geomechanics*, ASCE, **16**(2), 04015042. https://doi.org/10.1061/(ASCE)GM.1943-5622.0000526

Lu, N. and Godt, J. (2008). "Infinite slope stability under steady unsaturated seepage conditions." *Water Resources Research*, **44**(11), W11404. https://doi.org/10.1029/2008WR006976

Michalowski, R.L. and Drescher, A. (2009). "Three-dimensional stability of slopes and excavations." *Géotechnique*, **59**(10), 839-850. https://doi.org/10.1680/geot.8.P.136

Michalowski, R.L. and Nadukuru, S.S. (2013). "Three-dimensional limit analysis of slopes with pore pressure." *Journal of Geotechnical and Geoenvironmental Engineering*, ASCE, **139**(9), 1604-1610. https://doi.org/10.1061/(ASCE)GT.1943-5606.0000867

Nian, T.K., Chen, G.Q., and Luan, M.T. (2008). "Limit analysis of the stability of slopes reinforced with piles against landslide in nonhomogeneous and anisotropic soils." *Canadian Geotechnical Journal*, **45**(8), 1092-1103. https://doi.org/10.1139/T08-042

Oh, S. and Lu, N. (2015). "Slope stability analysis under unsaturated conditions: Case studies of rainfall-induced failure of cut slopes." *Engineering Geology*, **184**, 96-103. https://doi.org/10.1016/j.enggeo.2014.11.007

Pan, Q.J. and Dias, D. (2018). "Three dimensional face stability

of a tunnel in weak rock masses subjected to seepage forces." *Tunnelling and Underground Space Technology*, **71**, 555-566. https://dx.doi.org/10.1016/j.tust.2017.11.003

Pan, Q.J., Jiang, Y.J., and Dias, D. (2017). "Probabilistic stability analysis of a three-dimensional rock slope characterized by the Hoek-Brown failure criterion." *Journal of Computing in Civil Engineering*, ASCE, **31**(5), 04017046. https://doi.org/10.1061/(ASCE)CP.1943-5487.0000692

Qi, S.C., and Vanapalli, S.K. (2015). "Hydro-mechanical coupling effect on surficial layer stability of unsaturated expansive soil slopes." *Computers and Geotechnics*, **70**, 68-82. https://doi.org/10.1016/j.compgeo.2015.07.006

Qin, C.B. and Chian, S.C. (2018). "New perspective on seismic slope stability analysis." *International Journal of Geomechanics*, ASCE, **18**(7), 06018013. https://doi.org/10.1061/(ASCE)GM.1943-5622.0001170

Stianson, J.R., Chan, D., and Fredlund, D.G. (2015). "Role of admissibility criteria in limit equilibrium slope stability methods based on finite element stresses." *Computers and Geotechnics*, **66**, 113-125. https://doi.org/10.1016/j.compgeo.2015.01.014

Vahedifard, F., Leshchinsky, B.A., Mortezaei, K., and Lu, N. (2015). "Active earth pressures for unsaturated retaining structures." *Journal of Geotechnical and Geoenvironmental Engineering*, ASCE, **141**(11), 04015048. https://doi.org/10.1061/(ASCE)GT.1943-5606.0001356

Vahedifard, F., Leshchinsky, D., Mortezaei, K., and Lu, N. (2016). "Effective stress-based limit-equilibrium analysis for homogeneous unsaturated slopes." *International Journal of Geomechanics*, ASCE, **16**(6), D4016003. https://doi.org/10.1061/(ASCE)GM.1943-5622.0000554

Vanapalli, S.K., Fredlund, D.G., Pufahl, D.E., and Clifton, A.W. (1996). "Model for the prediction of shear strength with respect to soil suction." *Canadian Geotechnical Journal*, **33**(3), 379-392. https://doi.org/10.1139/t96-060

Vilar, O.M. (2006). "A simplified procedure to estimate the shear strength envelope of unsaturated soils." *Canadian Geotechnical Journal*, **43**(10), 1088-1095. https://doi.org/10.1139/t06-055

Xu, J.S., and Yang, X.L. (2018). "Seismic stability analysis and charts of a 3D rock slope in Hoek–Brown media." *International Journal of Rock Mechanics and Mining Sciences*, **112**, 64-76. https://doi.org/10.1016/j.ijrmms.2018.10.005

Yeh, T.C. (1989). "One-dimensional steady-state infiltration in heterogeneous soils." *Water Resources Research*, **25**(10), 149-2158. https://doi.org/10.1029/WR025i010p02149

Zhang, L.L., Fredlund, D.G., Fredlund, M.D., and Wilson, G.W. (2014). "Modeling the unsaturated soil zone in slope stability analysis." *Canadian Geotechnical Journal*, **51**(12), 1384-1398. https://doi.org/10.1139/cgj-2013-0394

APPENDIX A

$$f_1=\frac{1}{2}\left[e^{(\theta-\theta_0)\tan\varphi}+\frac{r_0'}{r_0}e^{-(\theta-\theta_0)\tan\varphi}\right] \tag{A1}$$

$$f_2=\frac{1}{2}\left[e^{(\theta-\theta_0)\tan\varphi}-\frac{r_0'}{r_0}e^{-(\theta-\theta_0)\tan\varphi}\right] \tag{A2}$$

$$f_3=\frac{\sin\theta_0}{\sin\theta}-\frac{1}{2}\left[e^{(\theta-\theta_0)\tan\varphi}+\frac{r_0'}{r_0}e^{-(\theta-\theta_0)\tan\varphi}\right]=\frac{\sin\theta_0}{\sin\theta}-f_1 \tag{A3}$$

$$f_4=\frac{\sin\theta_0\sin(\theta_B+\beta_1)}{\sin\theta_B\sin(\theta+\beta_1)}-\frac{1}{2}\left[e^{(\theta-\theta_0)\tan\varphi}+\frac{r_0'}{r_0}e^{-(\theta-\theta_0)\tan\varphi}\right]$$
$$=\frac{\sin\theta_0\sin(\theta_B+\beta)}{\sin\theta_B\sin(\theta+\beta)}-f_1 \tag{A4}$$

$$f_5=\frac{1}{3(1+9\tan^2\varphi)}[(3\tan\varphi\cos\theta_h+\sin\theta_h)\,e^{3(\theta_h-\theta_0)\tan\varphi}$$
$$-(3\tan\varphi\cos\theta_0+\sin\theta_0)] \tag{A5}$$

$$f_6=\frac{1}{6}\frac{L}{r_0}\left(2\cos\theta_0-\frac{L}{r_0}\right)\sin\theta_0 \tag{A6}$$

$$f_7=\frac{1}{6}e^{(\theta_h-\theta_0)\tan\varphi}\left[\sin(\theta_h-\theta_0)-\frac{L}{r_0}\sin\theta_h\right]\left[\cos\theta_0\right.$$
$$\left.-\frac{L}{r_0}+\cos\theta_h\,e^{(\theta_h-\theta_0)\tan\varphi}\right] \tag{A7}$$

$$g_1=2\int_{\theta_0}^{\theta_B}\int_0^{\alpha_1^*}f_2(f_1+f_2\cos\alpha)^2\,d\alpha d\theta$$
$$=\int_{\theta_0}^{\theta_B}f_2(2f_1^2+f_2^2)arc\cos(f_3/f_2)\,d\theta$$
$$+\int_{\theta_0}^{\theta_B}f_2(4f_1+f_3)\sqrt{f_2^2-f_3^2}\,d\theta \tag{A8}$$

$$g_2=2\int_{\theta_0}^{\theta_B}\int_0^{\alpha_1^*}f_2^2(\cos\alpha-\cos\alpha_1{}^*)(f_1+f_2\cos\alpha)^2\sin\theta\,d\alpha d\theta$$
$$=\int_{\theta_0}^{\theta_B}\left[arc\cos(f_3/f_2)(2f_1f_2^3-2f_1^2f_2f_3-f_2^3f_3)\right.$$
$$\left.+\sqrt{f_2^2-f_3^2}\left(2f_1^2f_2-2f_1f_2f_3+\frac{4}{3}f_2^3-\frac{1}{3}f_2f_3^2\right)\right]\sin\theta d\theta \tag{A9}$$

$$g_3=2\int_{\theta_B}^{\theta_h}\int_0^{\alpha_2^*}f_2(f_1+f_2\cos\alpha)^2\,d\alpha d\theta$$
$$=\int_{\theta_B}^{\theta_h}f_2(2f_1^2+f_2^2)arc\cos(f_4/f_2)d\theta$$
$$+\int_{\theta_B}^{\theta_h}f_2(4f_1+f_4)\sqrt{f_2^2-f_4^2}\,d\theta \tag{A10}$$

$$g_4=2\int_{\theta_B}^{\theta_h}\int_0^{\alpha_2^*}f_2(f_1+f_2\cos\alpha)^2f_6\,d\alpha d\theta$$
$$=\int_{\theta_B}^{\theta_h}f_2f_6(2f_1^2+f_2^2)arc\cos(f_4/f_2)d\theta$$
$$+\int_{\theta_B}^{\theta_h}f_2f_6(4f_1+f_4)\sqrt{f_2^2-f_4^2}\,d\theta \tag{A11}$$

$$g_5=2\int_{\theta_B}^{\theta_h}\int_0^{\alpha_2^*}f_2^2(\cos\alpha-\cos\alpha_2{}^*)(f_1+f_2\cos\alpha)^2\sin\theta\,d\alpha d\theta$$
$$=\int_{\theta_B}^{\theta_h}\left[arc\cos(f_4/f_2)(2f_1f_2^3-2f_1^2f_2f_4-f_2^3f_4)\right.$$
$$\left.+\sqrt{f_2^2-f_4^2}\left(2f_1^2f_2-2f_1f_2f_4+\frac{4}{3}f_2^3-\frac{1}{3}f_2f_4^2\right)\right]\sin\theta d\theta \tag{A12}$$

$$g_6 = \frac{b}{H}\frac{1}{2\tan\varphi}\left[e^{(\theta_h-\theta_0)\tan\varphi}\sin\theta_h - \sin\theta_0\right]\left\{\exp\left[2(\theta_h-\theta_0)\tan\varphi\right]-1\right\} \tag{A13}$$

$$\begin{aligned} g_7 = &-\frac{b}{H}\frac{1}{2\tan\varphi}\left[e^{(\theta_h-\theta_0)\tan\varphi}\sin\theta_h - \sin\theta_0\right]\sin\theta_0\left\{\exp\left[2(\theta_h-\theta_0)\tan\varphi\right]-1\right\} \\ &+\frac{b}{H}\left[e^{(\theta_h-\theta_0)\tan\varphi}\sin\theta_h - \sin\theta_0\right]\frac{3\tan\varphi\left\{\sin\theta_h\exp\left[3(\theta_h-\theta_0)\tan\varphi\right]-\sin\theta_0\right\}+\cos\theta_0-\cos\theta_h\exp\left[3(\theta_h-\theta_0)\tan\varphi\right]}{9\tan^2\varphi} \end{aligned} \tag{A14}$$

$$\begin{aligned} g_8 = &2\int_{\theta_0}^{\theta_B}\left[(f_2^2 f_3/8 - f_3^3/4 - 2f_1f_3^2/3 - f_3f_1^2/2 + 2f_1f_2^2/3)\sqrt{f_2^2-f_3^2} + (f_2^4/8 + f_2^2f_1^2/2)\arcsin(\sqrt{f_2^2-f_3^2}/f_2)\right]\cos\theta d\theta \\ &+2\int_{\theta_B}^{\theta_h}\left[(f_2^2 f_4/8 - f_4^3/4 - 2f_1f_4^2/3 - f_4f_1^2/2 + 2f_1f_2^2/3)\sqrt{f_2^2-f_4^2} + (f_2^4/8 + f_2^2f_1^2/2)\arcsin(\sqrt{f_2^2-f_4^2}/f_2)\right]\cos\theta d\theta \end{aligned} \tag{A15}$$

$$g_9 = \frac{b}{H}(f_5 - f_6 - f_7)\left[\sin\theta_h e^{(\theta_h-\theta_0)\tan\varphi} - \sin\theta_0\right] \tag{A16}$$